JGR Space Physics

RESEARCH ARTICLE
10.1029/2020JA028487

Electron Dropout Events and Flux Enhancements Associated With Geomagnetic Storms Observed by PROBA-V/Energetic Particle Telescope From 2013 to 2019

V. Pierrard[1,2], E. Botek[1], J.-F. Ripoll[3,4], and G. Cunningham[5]

[1]Royal Belgian Institute for Space Aeronomy, STCE and Space Physics, Brussels, Belgium, [2]Center for Space Radiations (CSR) and Georges Lemaître Centre for Earth and Climate Research (TECLIM), Université Catholique de Louvain (UCLouvain), Earth and Life Institute (ELI), Louvain-La-Neuve, Belgium, [3]CEA, DAM, DIF, Arpajon, France, [4]UPS, CEA, LMCE, Bruyères-le-Châtel, France, [5]Space Science and Applications, ISR-1, Los Alamos National Laboratory, Los Alamos, NM, USA

Key Points:

- Electron >500 keV flux measured by Energetic Particle Telescope at Low Earth Orbit from 2013 to 2019 shows dropouts followed by enhancements during all geomagnetic storms
- The study shows that dropouts deplete the outer radiation belt down to a minimum L-shell related to disturbed storm time (Dst)
- Electron fluxes are enhanced in the slot down to an impenetrable barrier with a L-shell related to Dst and to the plasmapause position

Supporting Information:

- Supporting Information S1

Correspondence to:
V. Pierrard,
viviane.pierrard@aeronomie.be

Citation:
Pierrard, V., Botek, E., Ripoll, J.-F., & Cunningham, G. (2020). Electron dropout events and flux enhancements associated with geomagnetic storms observed by PROBA-V/Energetic Particle Telescope from 2013 to 2019. *Journal of Geophysical Research: Space Physics*, *125*, e2020JA028487. https://doi.org/10.1029/2020JA028487

Received 15 JUL 2020
Accepted 11 NOV 2020

Abstract Electron flux variations for $E > 500$ keV during geomagnetic storms are investigated using the Energetic Particle Telescope (EPT). This detector launched in May 2013 on board the satellite PROBA-V at an altitude of 820 km was designed to provide uncontaminated spectra of electrons, protons, and alpha particles. Electron flux dropout events are observed during the main phase of each storm and even during substorms: a rapid reduction of the electron flux is noted throughout the outer electron radiation belt at all energies above about 0.5 MeV on timescales of a few hours. The electron spectrograms measured by the EPT between 2013 and 2019 show that after each geomagnetic storm, dropout events are followed by a flux enhancement starting first at low L values, and reaching the slot or even the inner belt for the strongest storms. We determine the link between Disturbed Storm Time (Dst) and the minimum value of the L-shell where the dropouts deplete the outer belt, as well as the nonlinear relation between Dst and the minimum L-shell where the flux penetrates in the slot region or even the inner belt during the storms. Dropouts appear at all energies measured by EPT and penetrate down to $L{\sim}3.5$ for the strongest events. Dropouts are observed at Low Earth Orbit each time Dst has an inverted peak < -40 nT. Flux enhancements appear at lower L only for big storm events with Dst < -50 nT. They penetrate down to an impenetrable barrier with a minimum L-shell related to Dst and to the energy. For $E > 1$ MeV, this limit is also linked to the plasmapause position.

1. Introduction

Magnetospheric perturbations driven by the solar wind cause substantial fluctuations of outer belt electron fluxes over short timescales. Such events are called dropouts. During these depletion events, the electron flux > 0.1 MeV can drop by several orders of magnitude in less than a few hours, often during geomagnetic storms (Turner et al., 2012). Reeves et al. (2003) performed a pioneering study of the variations of 1.8–3.5 MeV electron fluxes to geomagnetic storms from 1989 through 2000. They found that 53% of the storms caused an enhancement of the fluxes of electrons at geosynchronous orbit in comparison to the prestorm flux, 19% caused a decrease in fluxes, while 28% resulted in no significant change of fluxes. Benck et al. (2013) also analyzed statistically electron flux observations from DEMETER and SAC-C at Low Earth Orbit (LEO) during quiet and disturbed periods and developed a transient observation-based particle (TOP) model.

Many storms were later studied with Van Allen Probes launched in September 2012 (cf. review of Ripoll et al., 2020 and more specifically, the introduction of Turner et al., 2019 for a review on studies dedicated to storms). Turner et al. (2019) made a very complete analysis of the flux evolution during 110 storms that occurred between September 2012 and September 2017. It complemented the study of Turner et al. (2015) in which the authors had analyzed 52 storms from September 2012 to February 2015. For 1.5 MeV electrons at $L = 6$, they found 39% of the storms resulted in an enhancement, 26% resulted in depletion, and 35% resulted in no significant change in relative levels of the prestorm and post storm electron fluxes. They also reported that MeV electrons had the highest occurrence of dropout mainly at $L > 4$. Moya et al. (2017) considered 78 storms between September 2012 and June 2016. They observed that more intense storms caused the radiation belt to move inward toward the Earth. For 1.8 MeV electrons at $L = 6$, they showed

Table 1
Energy Ranges Corresponding to Each Virtual Channel of the EPT Instrument for Electrons

Energy channels Ch	Electrons (MeV)
1	0.5–0.6
2	0.6–0.7
3	0.7–0.8
4	0.8–1.
5	1–2.4
6	2.4–8
7	8–20

Abbreviation: EPT, Energetic Particle Telescope.

45%, 32%, and 23% probability of enhancement, depletion, or no-change response, respectively. Katsavrias et al. (2019) made a statistical analysis of 8 dropouts and 20 enhancement events, due to Coronal Mass Ejections or Corotating Interaction Regions driven storms from September 2012 to April 2018, showing the variation dependence on the energy and L.

In the present work, we study storms with EPT/PROBA-V at 820 km from May 2013 to end December 2019. To expand on previous works made about storms, we consider here:

(1) how low in L do the flux dropouts extend (this will be called Lmin)
(2) how low in L are enhancements seen (this will be called Lm), and
(3) the relationship between the inner edge of the outer belt and the plasmapause location

Previous Energetic Particle Telescope (EPT) observations during storms were presented in Pierrard and Lopez Rosson (2016), Lopez Rosson and Pierrard (2017), and Pierrard et al. (2019). LEO observations allow to observe a storm with a ∼2 h period, which is a major advantage to observe fast dynamics, offering a measurement of a given field line each 30 min compared with equatorial observations of the NASA Van Allen Probes (noted RBSP in following, standing for Radiation Belt Storm Probes, the original name of the mission before its launch), for which a given field line is crossed every ∼4 h (Mauk et al., 2012).

2. PROBA-V/EPT Observations

The EPT instrument has been developed to obtain the best discrimination between the particle species and determine uncontaminated particle spectra useful for space weather predictions (Cyamukungu et al., 2014). The instrument includes a low-energy section, consisting of two silicon detectors, and a high-energy section composed of 10 Digital and Absorber Modules, each of these composed by a sheet of an absorber material and a silicon sensor. EPT was launched on May 7, 2013 to a LEO polar orbit at an altitude of 820 km onboard the ESA satellite PROBA-V with an inclination of 98,73°, an orbital rotation period of 101.21 min and 10:30 a.m. as nominal local time at the descending node (Pierrard et al., 2014). The detector measures the particle fluxes for 7 virtual channels for electrons, 11 channels for protons, and 11 channels for helium ions. Table 1 summarizes the different energy ranges corresponding to each virtual channel for electrons used in the present study.

The EPT detects the particles penetrating via the aperture cone with an opening angle of 52°. The EPT on board the PROBA-V satellite is oriented West when in daylight and oriented East when in eclipse. The angle between its boresight direction and the local magnetic field varies between 60° and 120°, that is, around 90°, when no off-pointing of PROBA-V is performed for specific operational reasons or some scientific investigations as for example pitch angle distribution studies (Borisov et al., 2014). The angle between the instrument boresight direction and the local magnetic field is assumed to give the average particle pitch-angle over the field-of-view in the inertial reference system. While a range of pitch angles is sampled within the field-of-view, Cunningham et al. (2020) found that the detector count rate appears to be dominated by electrons that mirror at the satellite location.

The McIlwain (1966) and local B-field strength are evaluated using the UNILIB v2.20 (http://trend.aeronomie.be/NEEDLE/unilib.html) implementation of the IGRF/Olsen-Pfitzer quiet-time magnetic field model.

Figure 1 illustrates the electron fluxes observed by EPT from May 21, 2013 (a few days after the launch on May 7, 2013) up to December 31, 2019 (horizontal axis) for Channel (Ch) 1 (500–600 keV) and Ch 5 (1–2.4 MeV), as a function of the McIlwain parameter L in Earth radii (vertical axis). The observed disturbed storm time (Dst) index is given in the bottom panel.

One can see that the flux in the inner belt is quite low in 2013 (except just after the launch), and increases significantly in 2015, starting in January 2015 and even more highly in March and July 2015 (Pierrard &

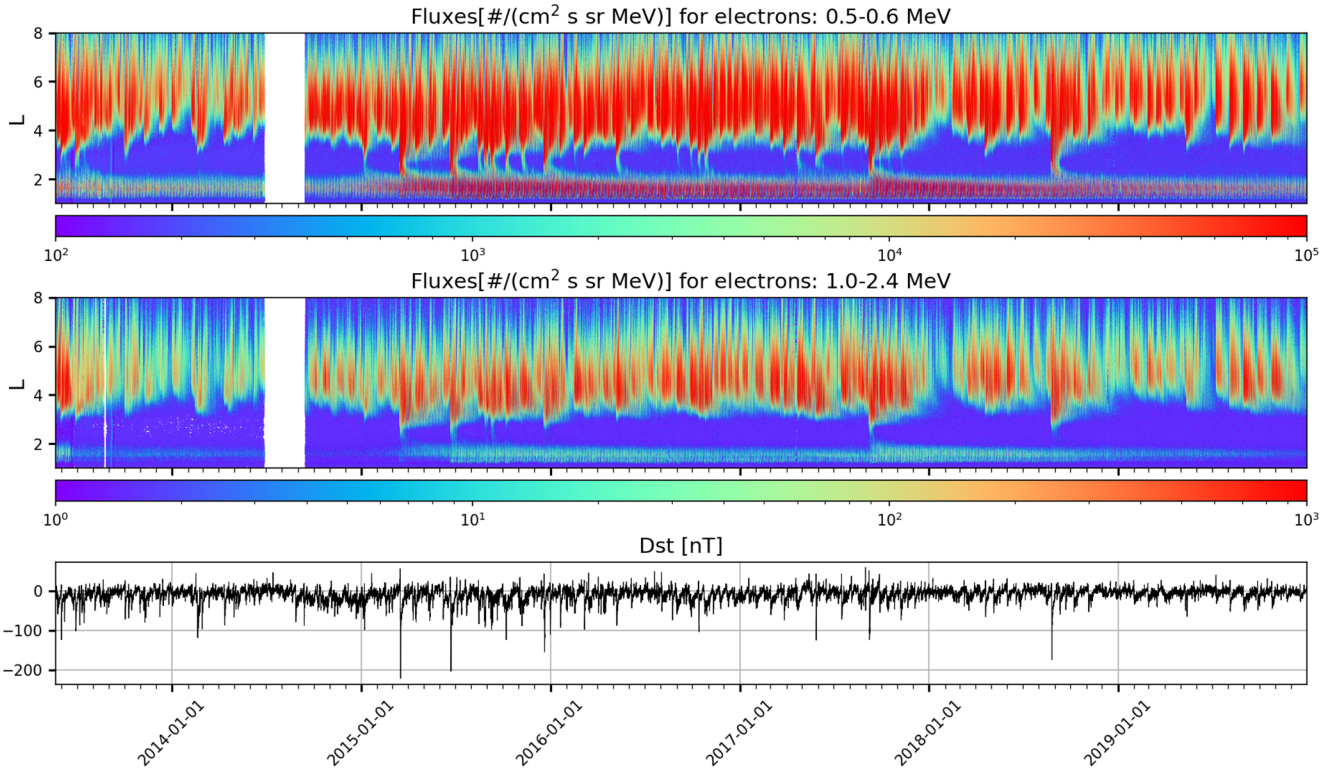

Figure 1. Electron fluxes observed by EPT from the first measurements on May 21, 2013 up to December 31, 2019, for Channel 1 (500–600 keV, upper panel) and Channel 5 (1–2.4 MeV, middle panel). The observed Dst index from January 1, 2013 is in the bottom panel. Dst, Disturbed Storm Time; EPT, Energetic Particle Telescope.

Lopez Rosson, 2016). Storms, characterized by inverted peaks of Dst, inject regularly 500 keV electrons in the inner belt, especially in 2015, and another big storm injected electrons in the inner belt in September 2017. Later, the storms do not reach the inner belt (except the one of August 26, 2018) and the inner belt flux decreases continuously during the last year. For the energy range (1–2.4) MeV, injections in the inner belt appear only during the strongest storms (Pierrard et al., 2019), that is, March 2015, June 2015, and September 2017, in good agreement with RBSP observations for similar energy (Claudepierre et al., 2019). The outer edge of the inner belt is energy-dependent. It is generally located at $L = 2$ (during low activity periods) for 500–600 keV and goes up to $L = 2.5$ after storms. The electrons remained trapped longer between $L = 2$ and $L = 2.5$ than at higher L. The slot region is fast formed again after the injection for L between 2.5 and 3.

Observations show that the inner and the outer electron radiation belt flux are the highest during the declining phase of the solar cycle 24 for which the peak of sunspots was in April 2014 (and minimum sunspots in end 2019), in association with fast solar wind streams, as previously noted for other solar cycles by Paulikas and Blake (1979). Note that EPT was not operational during 3 months from June to September 2014 (Pierrard et al., 2019).

The Dst index is obtained from the variations of the horizontal component of the terrestrial magnetic field observed in different stations located close to the equator at the surface of the Earth. Dst variations, often taken as indicator for geomagnetic storms, are mainly driven by the ring current basically composed of ions with energies of about 10–200 keV. More specifically, O^+ is a major component below 15 keV and H^+ dominates above about 100 keV. The main phase of a typical geomagnetic storm corresponds to the sharp decrease of Dst in a few hours due to ring current injection, which results from a southward Interplanetary Magnetic Field (IMF) and the resultant strong convection. The recovery phase corresponding to the progressive increase of Dst in a few days after Dst minimum is due to loss of ring-current ions as a result of charge exchange with the neutral exosphere. Although Dst is associated with flux variations of other ions and electrons of lower energy, it is also a good indicator for flux variations in the radiation belts.

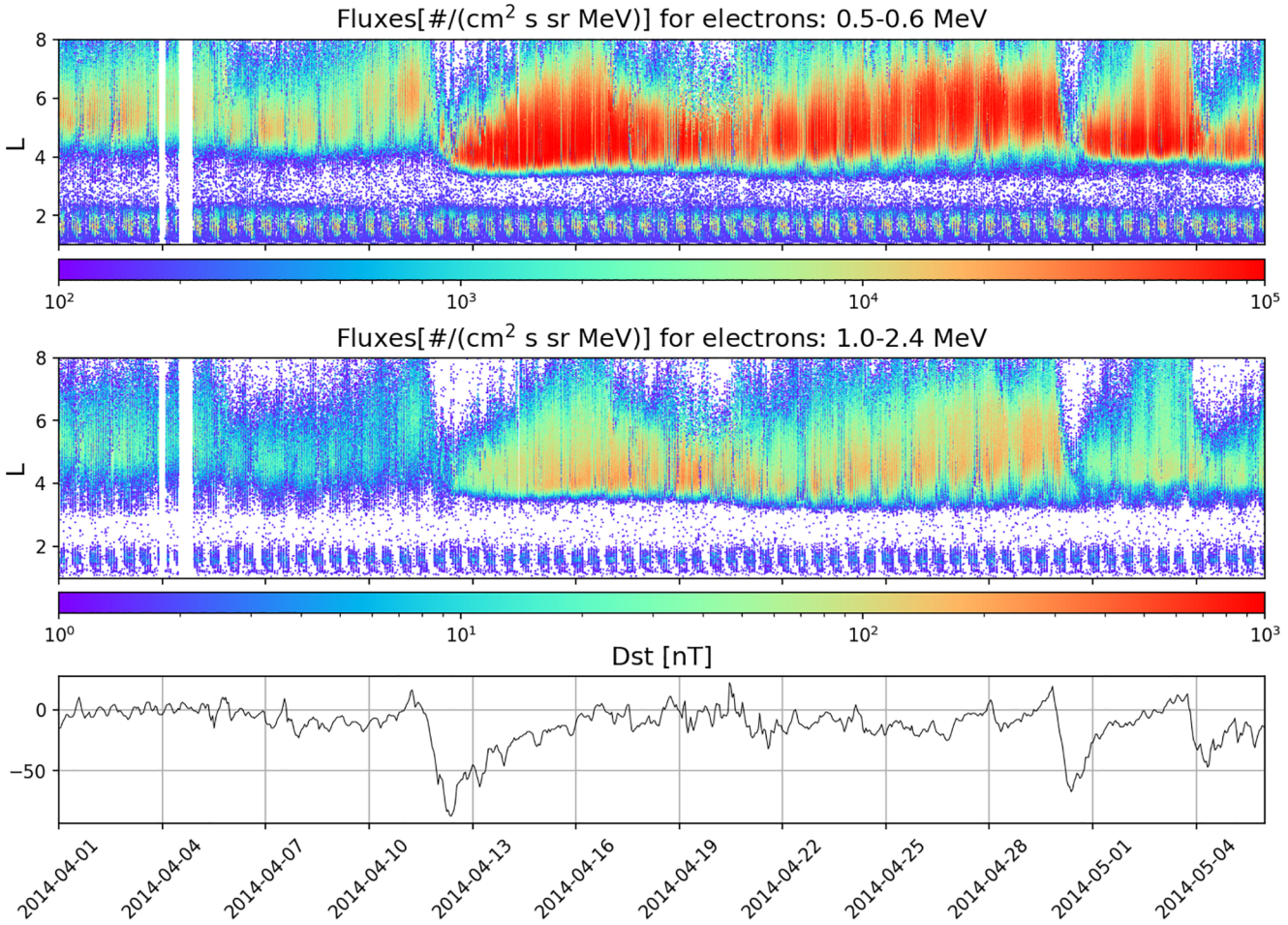

Figure 2. Electron flux observed by EPT from April 1, 2014 to May 6, 2014 for Channel 1 (500–600 keV, upper panel) and Channel 5 (1–2.4 MeV, middle panel). The observed Dst index is given in the bottom panel. Dst, Disturbed Storm Time; EPT, Energetic Particle Telescope.

3. Observations of Geomagnetic Storms: Dropouts and Flux Enhancements

3.1. Storm Observations

Typical examples of electron flux variations measured by EPT during several increasingly large geomagnetic storms are illustrated in Figures 2–4. Flux variations in the outer belt are directly related to the storms. Dropouts down to L∼4 appear during all geomagnetic perturbations, while flux enhancements at lower L-shells in the slot appear only after the strongest storms.

Figure 2 illustrates electron fluxes observed by PROBA-V/EPT from 500 to 600 keV (upper panel) and 1–2.4 MeV (middle panel) during the month of April 2014. The lower panel shows Dst. It can be observed that the flux in the outer belt is highly variable, especially at high L values. Two storms (April 12, 2014 with Dst = −80 nT and April 29, 2014 with Dst = −67 nT) can be noticed, associated with sharp flux decreases above $L = 4$. Another Dst min of −45 nT appears on 4 May and leads to a dropout at $L > 5$. Such dropout events are frequently observed. More than 6 years of EPT observations show that dropouts are well observable from LEO and appear in fact each time the Dst index has an inverted peak lower than −40 nT.

The dropout starts at high L with the main phase associated to the sharp decrease of Dst, and generally reaches its minimum L value a little bit before Dst is minimum (see Figure 5 for a zoom showing this with better resolution). Immediately after the dropout of the geomagnetic storm, the flux increases at lower L values than the dropout minimum L, where the particles are left, so that the inner edge of the outer belt penetrates deeper in the slot region for the biggest storms. Sudden particle enhancements appear after the

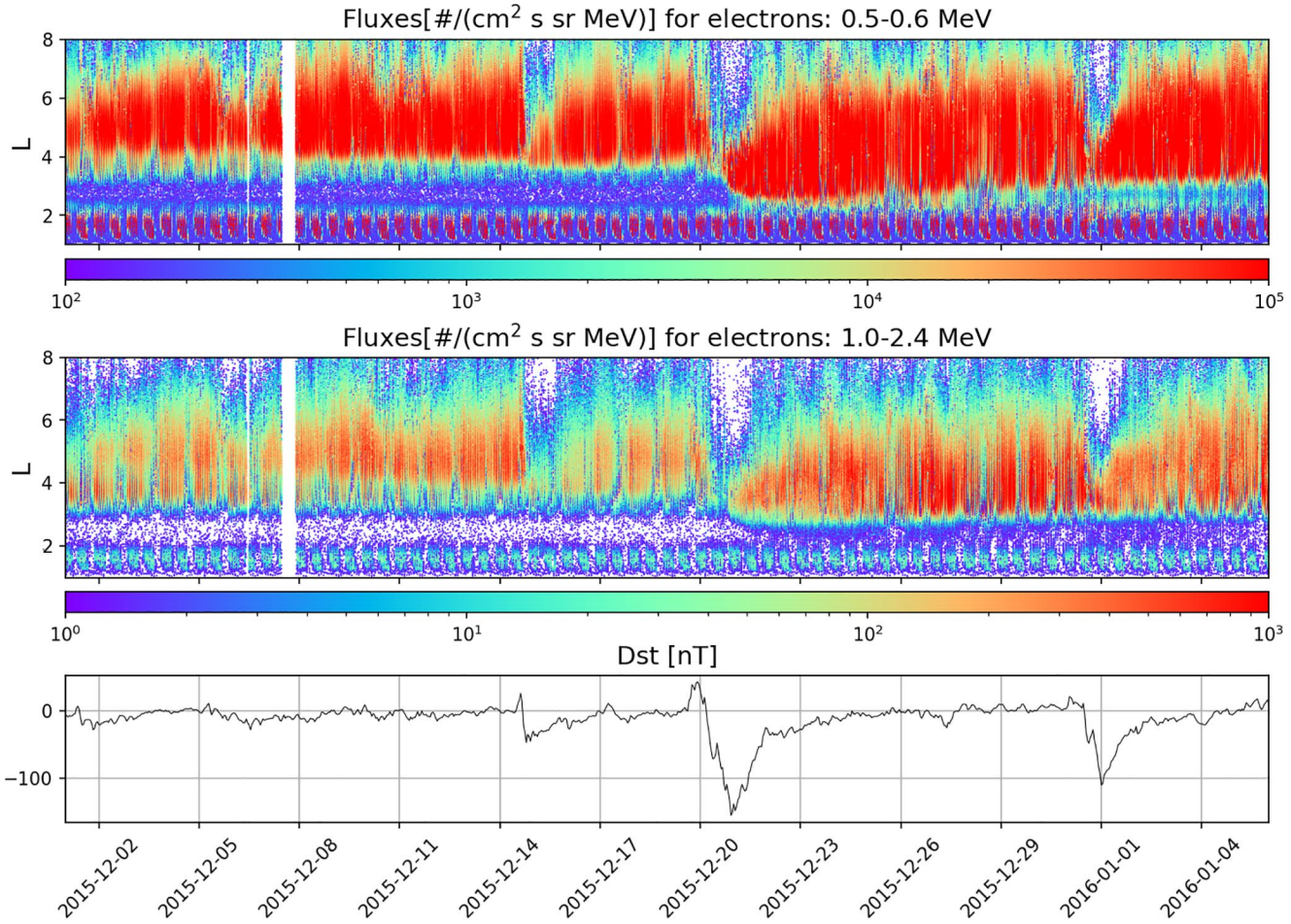

Figure 3. Dropouts observed from December 1, 2015 to January 6, 2016 by EPT/PROBA-V (on December 14, 21, 2015 and January 1, 2016) for Channel 1 (500–600 keV, upper panel) and Channel 5 (1–2.4 MeV, middle panel). Dropouts are observed for each geomagnetic storm with Dst lower than −50 nT (see bottom panel). The dropout is typically observed down to $L = 4$. Dst, Disturbed Storm Time; EPT, Energetic Particle Telescope.

inverted peak of Dst. The flux increase seems to follow the progressive recovery phase, with the lowest L regions refilled first and the higher L regions refilled as Dst increases, suggesting that Dst and L can be directly related.

Figure 3 is similar to Figure 2, but for the month of December 2015. Other dropouts are observed up to $L = 4$ and directly associated to Dst inverted peaks. Dst < -50 nT corresponds to the threshold often used to determine a geomagnetic storm. One can see that for the storm of December 20, 2015 (Dst min $= -155$ nT), the inner edge of the outer belt is pushed further inward than for the storm of April 12, 2014 (Dst min $= -80$), and even reaches the inner belt for Ch1. On the contrary, the smaller event of December 14, 2015 (Dst min ~ -50 nT) does not lead to an inward motion of the inner edge of the outer belt.

The biggest geomagnetic storms of the 24th solar cycle appeared in March 2015 (lowest Dst $= -223$ nT). This so-called St Patrick's Day storm is illustrated in Figure 4 for different EPT energy channels. The dropout is observed in all energy channels. The time progression of the dropout seems quite independent on the energies. After the dropout, the flux increases and penetrates at lower L in the slot region for all energies except those of $E > 2.4$ MeV for which the flux does not penetrate at $L < 2.6$. Baker et al. (2014) called this threshold an impenetrable barrier for ultrarelativistic electrons due to the weak radial diffusion at these energies. Even for the highest energy Ch6 ($E > 2.4$ MeV), there is a dropout and after that a flux enhancement in the slot region at lower L than before the storm, but reaching only $L > 2.6$.

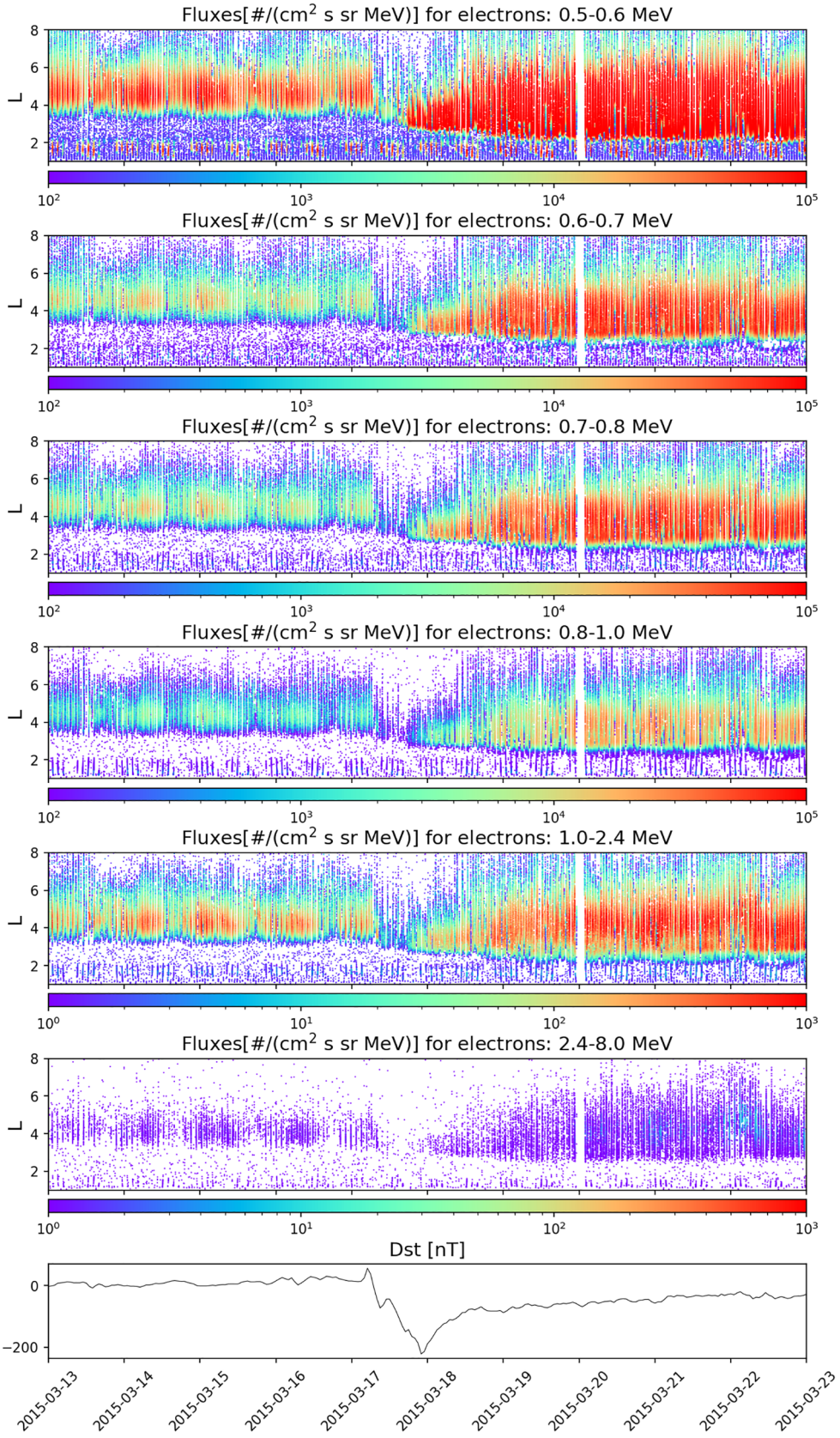

Figure 4. Electron fluxes observed by EPT from March 13, 2015 up to March 23, 2015, for the six energy channels. Dst is in the bottom panel. Dst, Disturbed Storm Time; EPT, Energetic Particle Telescope.

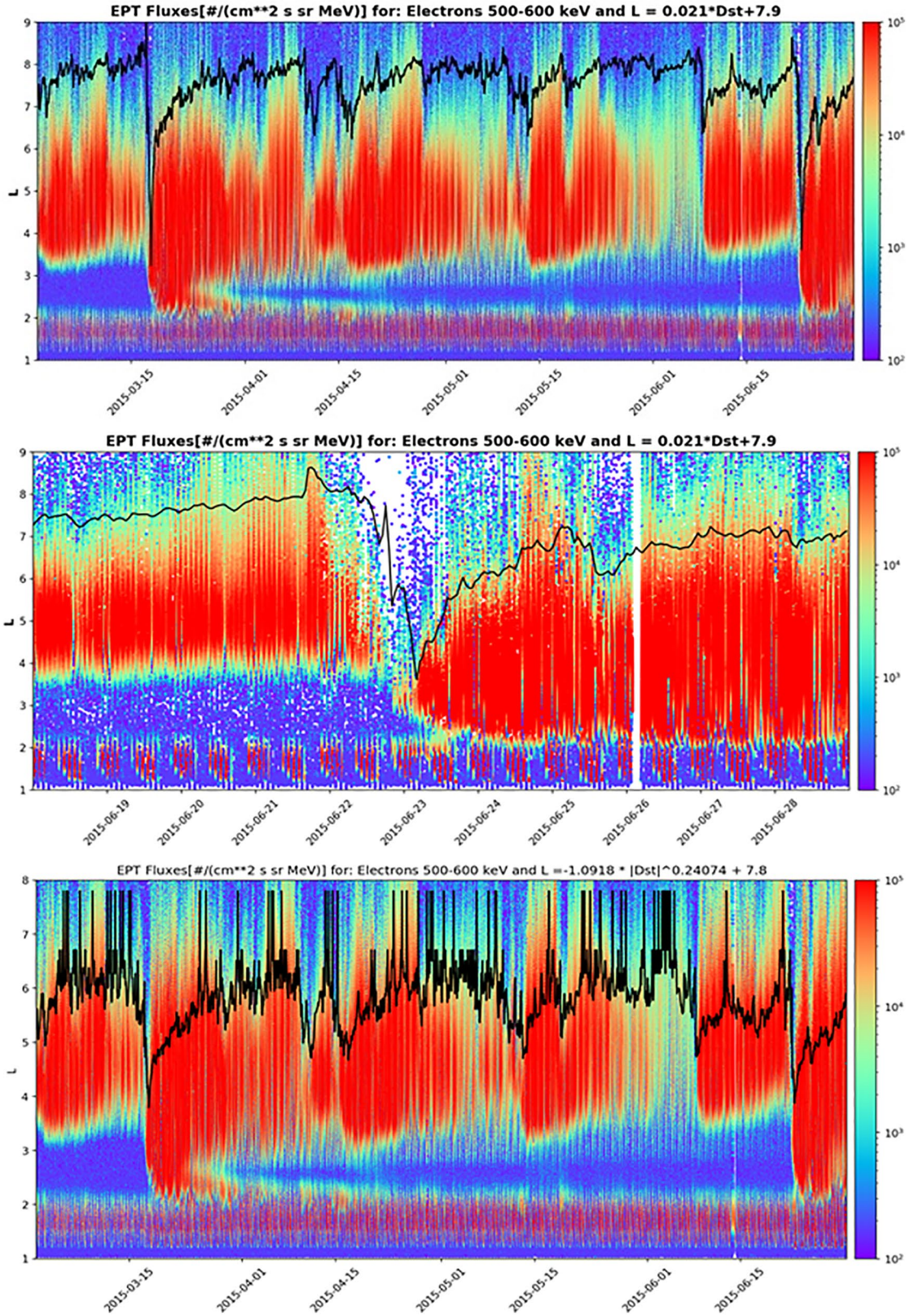

Figure 5. Electron flux observed by EPT from March 1 to June 30, 2015 (upper and bottom panel) and zoom from June 18, 2015 to June 28, 2015 (second panel), for Channel 1. A black line representing *L*min is superposed and corresponds to a linear relation based on the observed Dst index in the first and second panels, and to a power law obtained for Dst < −40 nT only in the bottom panel. Dst, Disturbed Storm Time; EPT, Energetic Particle Telescope.

Figure 5 (first panel) illustrates the electron flux observed by EPT from 1 March to 30 June 2015 in Ch 1, and the middle panel shows a zoom on the big storm of June 23, 2015 (Dst = −204 nT). Like for the other storms, when Dst is low, a dropout appears, indicating clearly a direct link between Dst and minimum value of L where fluxes are observed. A linear relation $L\text{min} = 0.021*\text{Dst} + 7.9$ is shown by the superposed black line in first and second panels of Figure 5 and clearly illustrates the relation between the outer edge of the outer belt and Dst, including during the dropouts and during the recovery phase. Note that this linear relation corresponds well to the outer edge of the belt during the recovery phase of the storms.

The minimum of dropout Lmin is identified by the L-shell above which the flux is lower than a threshold corresponding to 10^2 electrons/(cm^2 s st MeV) in the present case (appearing as dark blue in Figure 5). With this definition, Lmin corresponds to the outer edge of the outer belt. Lmin has to be distinguished from Lm, the inner edge of the outer belt that will be used later in the manuscript.

Even weak events due to small decreases of Dst show a dropout at high L. But the linear relation does not represent well the low L-shells obtained during such small Dst events. Using the minimum L-shell (Lmin) only during events with Dst < −40 nT (thus only during dropouts), the best relation is provided by a power law:

$L\text{min} = a\,|\text{Dst}|^b + c$ with $a = -1.0918$, $b = 0.24073559$, and $c = 7.8$ (illustrated and superposed to the EPT fluxes of Ch1 in the bottom panel). The behavior of this power law relation is better during the storms associated to Dst < −40 nT (thus, dropouts with Lmin < 5.15), but not between consecutive storms, and especially not during the recovery phase.

For Dst < −40 nT, the values of the minimum L-shell Lmin are generally located around $L = 4$, lower than the L-shell obtained by the linear relation. The power law relation gives better values of Lmin for small events and, contrary to the linear one, it remains valid for very big events with Dst < −250 nT, even if none of them are observed during the period of time used in the present analysis. The observed dropouts never reach the inner belt, which indicates an "impenetrable barrier" for the dropout down to the region where injections take place during storms. The magnetic field compression has somehow to be limited in L-shell, which creates this limit, a barrier under which dropouts cannot reach and depopulate the radiation belts electrons.

One can also observe in the middle panel of Figure 5 that the dropout of the June 22, 2015 starts during the Sudden Storm Commencement, thus, even before the Dst decrease. This is the case for many other storms (for instance the previous storm, also in June 2015, illustrated in Figure 5 top panel). That could be an indication that the dropout is not due to the modification of the magnetic field of the Earth (thus, not to the adiabatic invariant), but more due to magnetopause shadowing effect (see discussion later). In other cases, the dropout starts simultaneously with the Dst decrease (for instance on March 17, 2015 as illustrated in Figure 5 top panel), but the flux decrease is generally faster than the Dst decline. In all cases, the dropout has already reached the minimum Lmin value a few hours before Dst has reached its minimum value. The time delay corresponds approximately to the duration of the main phase.

For the strongest storms, such as that of June 22, 2015, the fluxes disappear above $L = 3.8$ at the beginning of the storm, while fluxes increase below (from $L = 2.8$ to $L = 3.8$ for this example) during the dropout. When Dst is minimum, the fluxes at $L > 3.8$ are still empty, but the fluxes below increase even more and penetrate in the slot region up to the inner belt. The minimum Lm value is reached by the inward push of the inner edge of the outer radiation belt a few hours after the minimum of Dst.

Note that the inner belt is only observed when the LEO satellite PROBA-V crosses the South Atlantic Anomaly (SAA) (Pierrard et al., 2014). Due to the pitch angle sampled changing over the SAA, flux values appear discontinuous for $L < 2$ on Figure 5 (especially middle panel). High fluxes in the SAA are due to the weak magnetic field intensity B in this region.

3.2. Study of Dropouts

The observations show that dropouts appear for all energy ranges and reach typically $L \sim 4$ when Dst is lower than −40 nT. Moreover, dropouts appear not only during geomagnetic storms, but they seem to be observed during each inverted peak of Dst. This is even better illustrated in Figure 6 with the fluxes as a

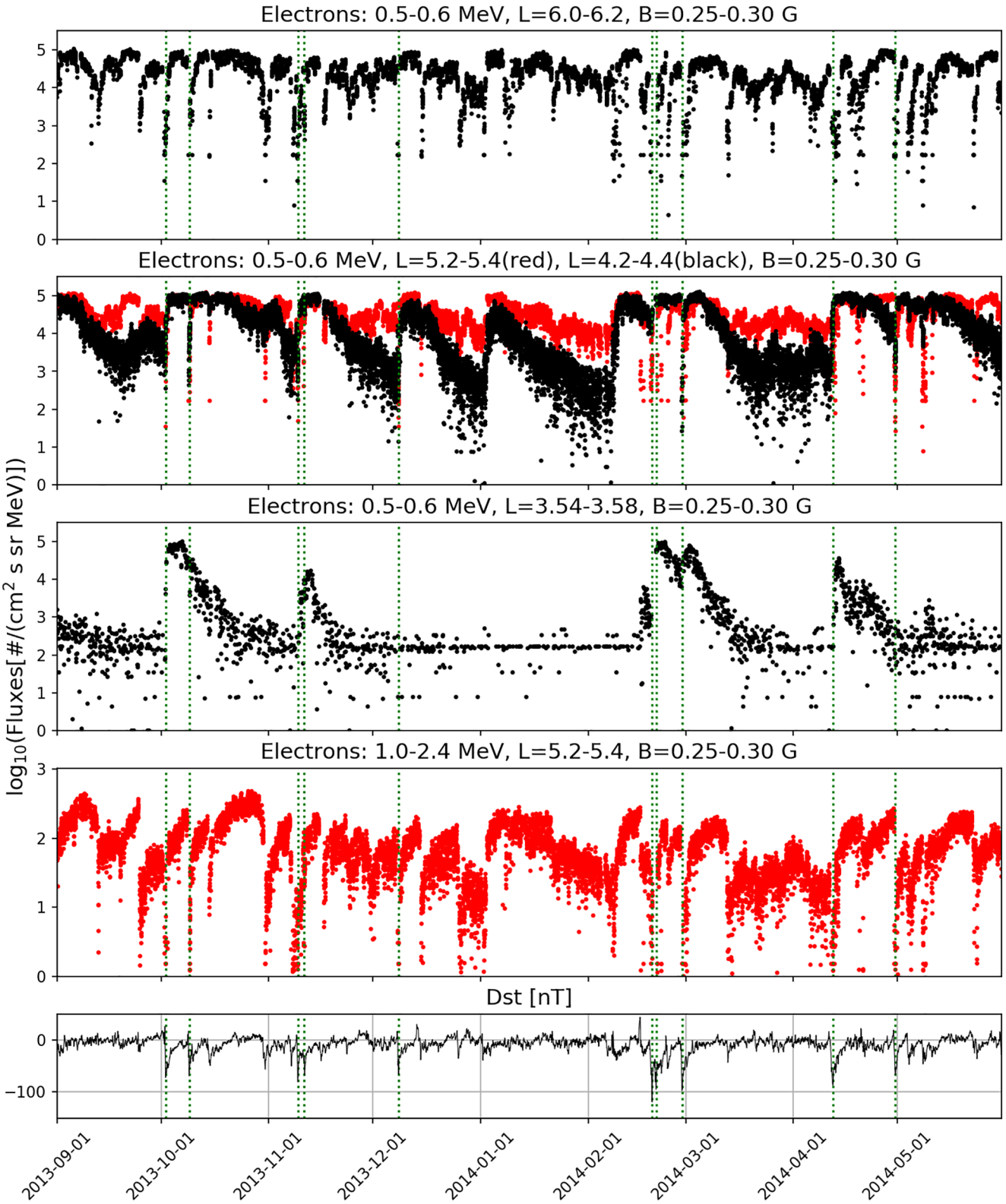

Figure 6. Electron flux observed by EPT as a function of time from September 1, 2013 to May 31, 2014 in Channel 1 (500–600 keV) in bin B = [0.25, 0.3] G and L = [6.0–6.2] Re (upper panel). Second panel: the same but for L = [5.2–5.4] Re (in red) and L = [4.2–4.4] Re (in black). The decay times are shorter at low L values. Third panel: the same but for L = [3.54–3.58] in the slot region. Fourth panel: the same as panel 2 (red line) but for Channel 5 (E = 1–2.4 MeV). Dst is shown in the bottom panel. Vertical green dotted lines indicate the strongest geomagnetic storms with Dst < −50 nT. Dst, Disturbed Storm Time; EPT, Energetic Particle Telescope.

function of time from September 1, 2013 to May 31, 2014 at $L = 6.1$ (upper panel), 5.3 (second panel in red), and 4.3 (second panel in black). On this figure, the data are sorted in bins depending not only on L, but also on B (here $B = [0.25,0.3]$ Gauss) to have temporal series of fluxes located always at the same position, following Pierrard et al. (2019).

One can see that the dropouts are present not only for ultrarelativistic electrons (fourth panel of Figure 6 for Ch 5 from 1 to 2.4 MeV), but already for energies of 500 keV (panels 1–3 for Ch1 from 500 to 600 keV). They are more frequent at high L values while at $L < 4.4$, only the biggest storms with Dst < -40 nT are associated to dropouts, as visible in the second panel of Figure 6 by comparing the red and black dots marking the low fluxes observed during dropouts at $L = 5.3$ and $L = 4.3$ respectively. At $L = 6.1$, dropouts already appear at each inverted peak of Dst < -25 nT and they stay confined to high L. Strongest storms with Dst < -50 nT are indicated by the green vertical dotted line in the panels of Figure 6.

Xiang et al. (2017) noted with RBSP data that the storm of February 27, 2014 showed dropout at $L < 6$, but not at $L > 6$. This is not observed with EPT in Figure 6.

Immediately after the dropouts, the flux increases at all $L > 4$. It takes values around 10^5 electrons cm^{-2} s^{-1} sr^{-1} MeV^{-1} for Ch 1, which seems to be a maximum in the outer belt during this period of time. Note that 10^6 values are frequently observed in Ch 1 during the more active year of 2015. For Ch 5 (fourth panel of Figure 6), the maximum flux reached after the storm is more variable than for Ch 1.

The flux is generally higher after the storm in comparison to the prestorm flux, mainly depending on the dates of the previous storms. If there is more than one month between two storms (as for instance in February 2014), the flux before the storm is quite low because it slightly decreases with time during quiet periods. The flux after the storm is then much higher than before the dropout, especially at low L where the flux decreases faster with time during quiet periods. If a previous storm appeared only a few days before the new storm (as it is, e.g., the case in October 2013 or in February 2014), the flux is almost the same after as before the dropout. For Ch5 (Figure 5 fourth panel), the flux continues to increase several days after the storm.

Note that there are small events in January and February 2014 for instance with a Dst around −40 nT (>−50 nT, thus, not indicated by a green dotted line in Figure 6) that show a behavior similar to stronger storms. There are other events with similar Dst (for instance in March 2014) where the flux is lower than before the storm. The flux behavior of such small events with Dst > -50 nT is, thus, more difficult to characterize than for the biggest storms.

At $L = 4.3$ (black points of second panel of Figure 6), the dropouts are less visible (due to the low flux after long quiet periods), but the flux increase associated to the most important Dst events becomes more noticeable. After the storms and during quiet periods, the flux slightly decreases with time during quiet periods with lifetimes dependent on L. This is likely associated to wave-particle interactions with whistler-mode hiss waves (Ripoll et al., 2016, 2017, 2019). The decay times after the flux enhancements are clearly shorter at $L = 4.3$ than at $L = 5.3$, as illustrated on the second panel of Figure 6, so that the dropouts are more visible at high L values where the fluxes remain high during quiet periods. This electron flux decay is exponential, with a lifetime of a few days. Note that the lifetimes derived from other LEO observations by Benck et al. (2010) were all around 5 days for $L > 3.5$. The lifetimes are energy-dependent and vary between 1 and 20 days in the slot and the outer zone when observed from the Van Allen Probes (Claudepierre et al., 2020a). MagEIS lifetimes from Claudepierre et al. (2020a) (their Figure 1) are in qualitative agreement with pitch angle scattering from hiss waves for a large range of (L, E) (Claudepierre et al., 2020b; Ripoll et al., 2019).

3.3. Study of Flux Enhancements

While the flux drops in the outer belt ($L > 4$ typically), the flux increases at $L < 4$ (in fact, at some $L < L$min of the dropout) during main storms because new particles are injected at lower L, as illustrated for $L = 3.56$ in Figure 6 (third panel) for EPT for the time period from September 2013 to May 2014. The lower Dst, the lower the minimum L shell (Lm) where electrons are injected. For $L < 4$ (often corresponding to the edge of the outer belt and the slot region), the flux increases during each geomagnetic storm considered as the cases for which Dst < -50 nT, but the deepness of Lm depends on Dst. For low energies (10–100 keV), not

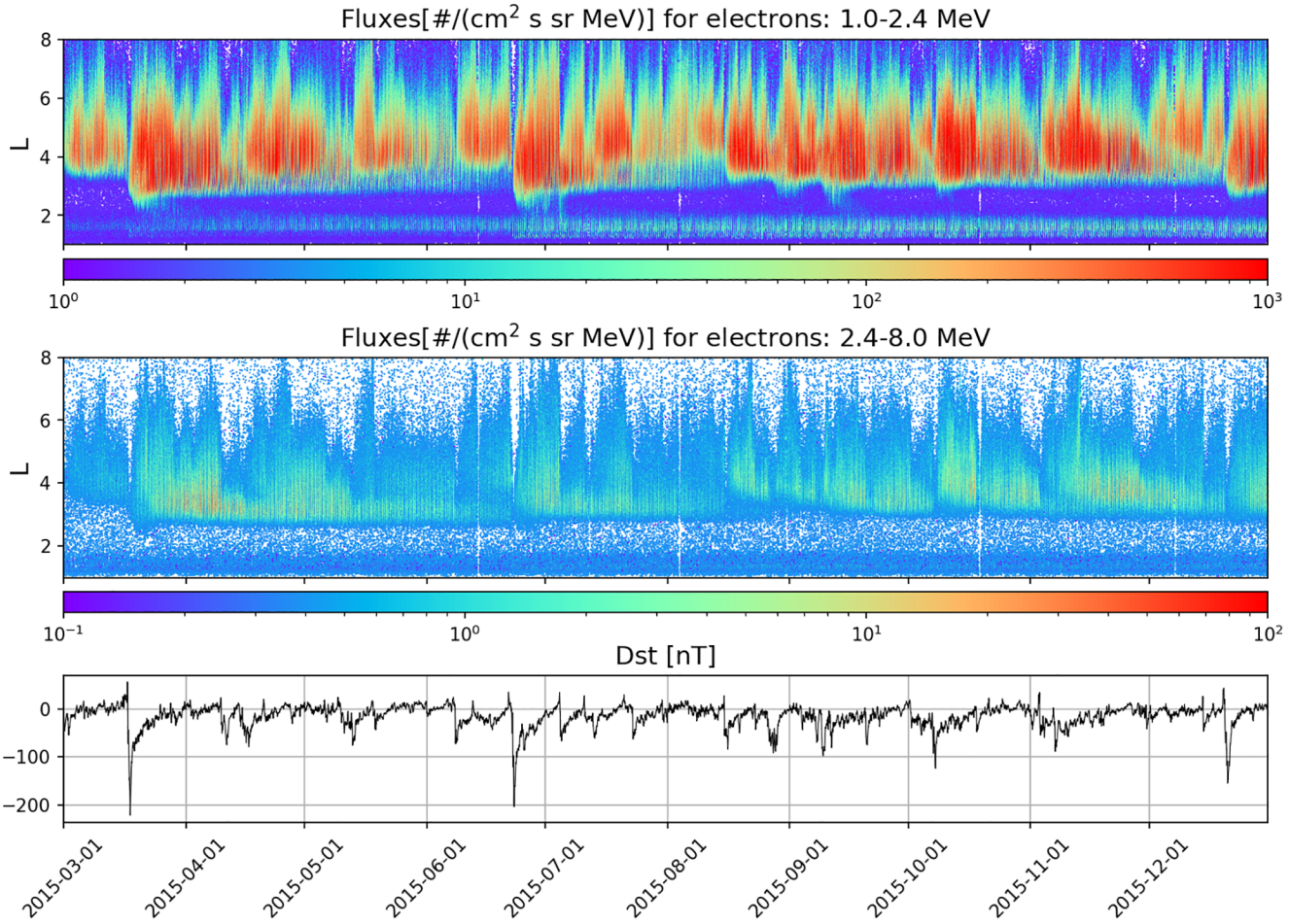

Figure 7. Relativistic and ultrarelativistic electron flux observed by EPT during 2015 in Channel 5 (1–2.4 MeV, upper panel) and Channel 6 (2.4–8 MeV, second panel). Dst is given in the bottom panel. Dst, Disturbed Storm Time; EPT, Energetic Particle Telescope.

observed by EPT, injections can occur between $L = 2.5$ and 4.5 depending on geomagnetic conditions and MLT (Turner et al., 2015). In that case, frequent penetrations from the outer belt down to the inner belt are observed (e.g., Reeves et al., 2003), itself with its outer edge reaching higher L-shell (L~3.5 for 100 keV in Ripoll et al. [2019]).

Figure 7 shows that flux penetrations in the slot are present also at high energies. For 1–2.4 MeV (upper panel), fluxes penetrate down to the inner belt during the main storms (Pierrard et al., 2019) and are lost after several days, likely due to pitch angle scattering from hiss waves, recreating the slot between the two belts, first around $L = 2.5$ and after months of quiet days between $L = 2$ and $L = 3$. For higher energies (>2.4 MeV, Ch 6, middle panel of Figure 8), the flux does not penetrate lower than $L = 2.8$ in agreement with Baker et al. (2014). During the 6-year observations, there are no very big storms with Dst < −230 nT, while this conclusion could be different for bigger storms. Penetrations as low as Lm = 2 were observed by SAMPEX for 2 MeV electrons during some of the 11 storms with Dst < −230 nT observed between 1999 and 2005 (Zhao & Li, 2013), although SAMPEX MeV measurements have suffered some corruption by lower energy electrons (Selesnick, 2015). This reinforces the need of uncontaminated MeV measurements at low L-shell. Between October 1999 and May 2005, four storms had a minimum Dst < −300 nT.

The depth of electron penetration is correlated with the storm strength as measured by the minimum of Dst, as seen in Figure 7 for relativistic and ultrarelativistic electrons. This appears also clearly in Figure 8 where the electron fluxes observed by EPT from May 7, 2013 to December 31, 2019 in Channel 1 (500–600 keV)

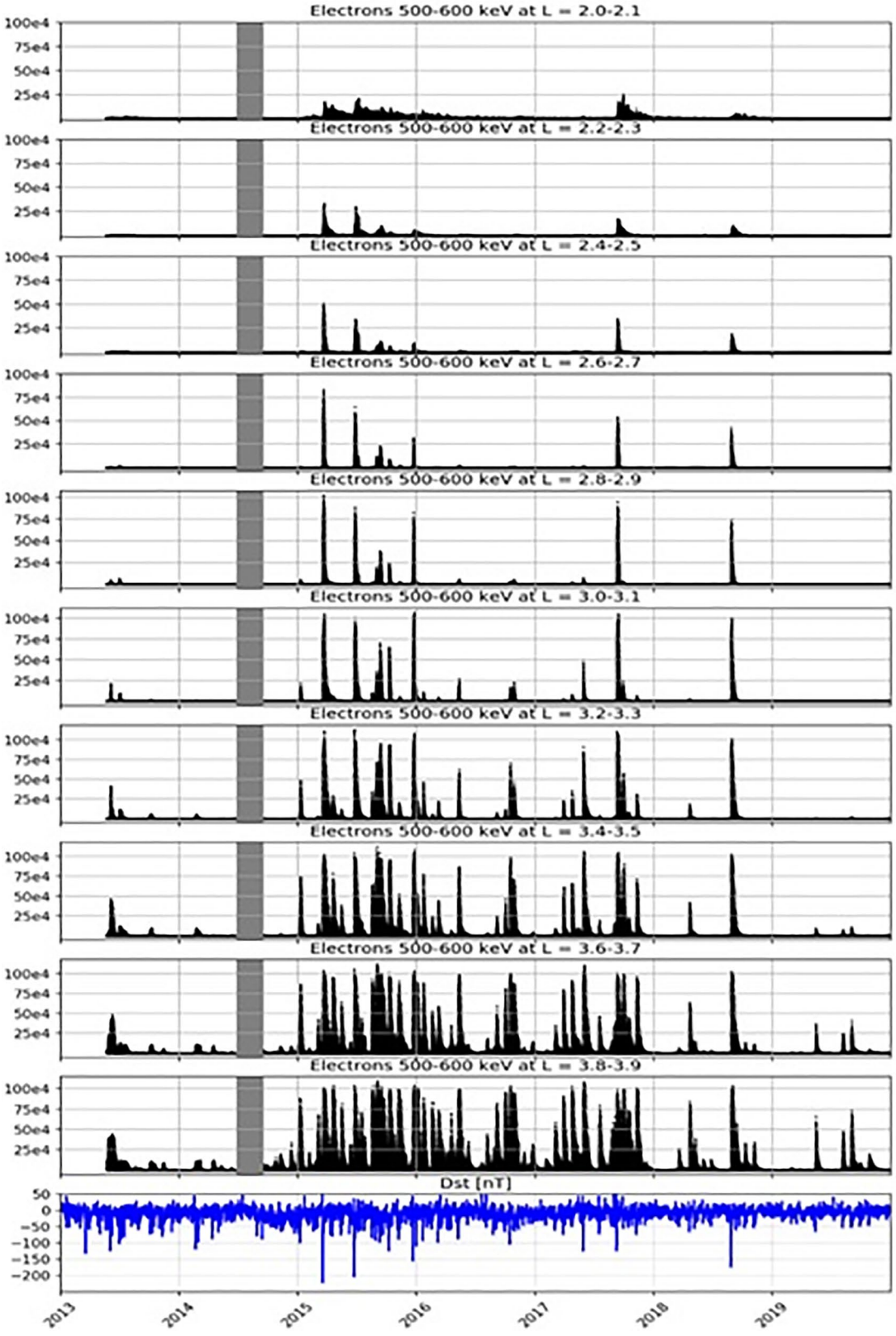

Figure 8. Electron flux in electrons/(cm^2 s sr MeV) observed by EPT from May 7, 2013 to December 31, 2019 in Channel 1 (500–600 keV) for bins in L increasing by steps of 0.1 from $L = 2.0$ to $L = 3.9$. In the slot region, the flux increases during the most important storms, and the deepness depends on Dst (bottom panel). Dst, Disturbed Storm Time; EPT, Energetic Particle Telescope.

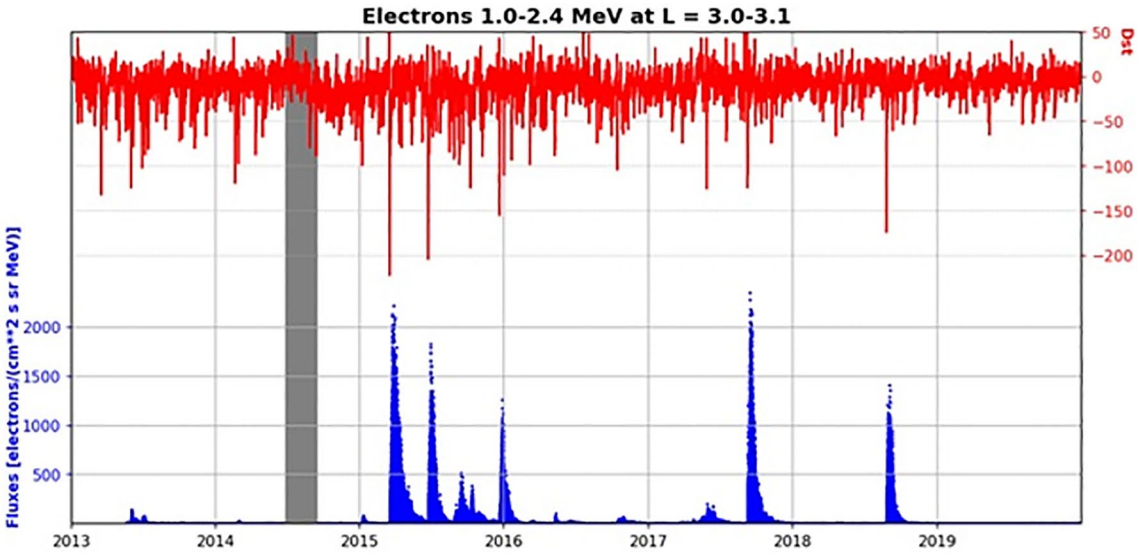

Figure 9. Electron flux in Ch 5 (1–2.4 MeV) in L = 3–3.1 during the same period from May 7, 2013 to December 31, 2019. The gray shaded region marks the missing data window from June to September 2014.

are shown in bins located in the slot region ranging from very low $L = 2.0$ up to higher $L = 3.9$ with an increasing step delta $L = 0.1$.

In the slot, the fluxes are close to zero except during the most important storms and following days. The deepness of the injection depends on Dst that is illustrated in the bottom panel of Figure 8. Between $L = 2.2$ and 2.3 for instance (second panel of Figure 8), only the biggest storms have injected fluxes. Taking for instance a threshold of 25.e4 electrons/(cm^2 s sr MeV), only two storms reached these low L values during the 6 years of observations. In the range $L = 2.4$–2.5 (third panel of Figure 8) and three storms are observed (one more) and five storms (two more) in $L = 2.6$–2.7 (fourth panel), using the same threshold. This technique allows us to obtain an automatic process to determine Lm as a function of Dst for all storms with Dst < -50 nT between May 2013 and December 2019. We look at a window of a few days that includes Dst min and determine whether some threshold in flux is crossed during that window. The thresholds used in the automatic process are 5.e4 electrons/(cm^2 s sr MeV) for Ch 1 and 2.e2 electrons/(cm^2 s sr MeV) for Ch 5. They correspond to the limits for which the effects of storms can clearly be identified. Note the higher flux observed at $L = 2$–2.1 than at 2.2–2.3, due to the fact that $L = 2$ corresponds to the limit between the slot and the inner belt.

The value of Lm is energy dependent. The same method allows us to determine Lm of the flux injections as a function of Dst for all energies. An example of what is found for Ch 5 (1–2.4 MeV) in $L = [3–3.1]$ is represented in Figure 9 (to compare panel 6 of Figure 8 for Ch 1).

Figure 10 illustrates the minimum Lm values of the L-shell of the flux injections versus Dst for Ch 1 (500–600 keV, upper panel) and Ch 5 (1–2.4 MeV, bottom panel) for the storms with Dst < -50 nT observed during the period of 7 May to 31 December 2019.

Among the 50 storms appearing between May 2013 and December 2019, a few are not covered by EPT (June–September 2014) or they do not reach Lm in the range shown in Figure 10.

For low energies (500–600 keV) (top panel of Figure 10), one can see a clear nonlinear dependence of Lm as a function of Dst. Indeed, Lm reaches several times $L = 2.2$, always for the four events with Dst < -125 nT. For less strong storms ($-50 <$ Dst < -125 nT), the spread is higher but Lm is generally proportional to the Dst. For electrons with $E < 1$ MeV, flux enhancements at $L < 2.6$ occur several times even under moderate geomagnetic activity

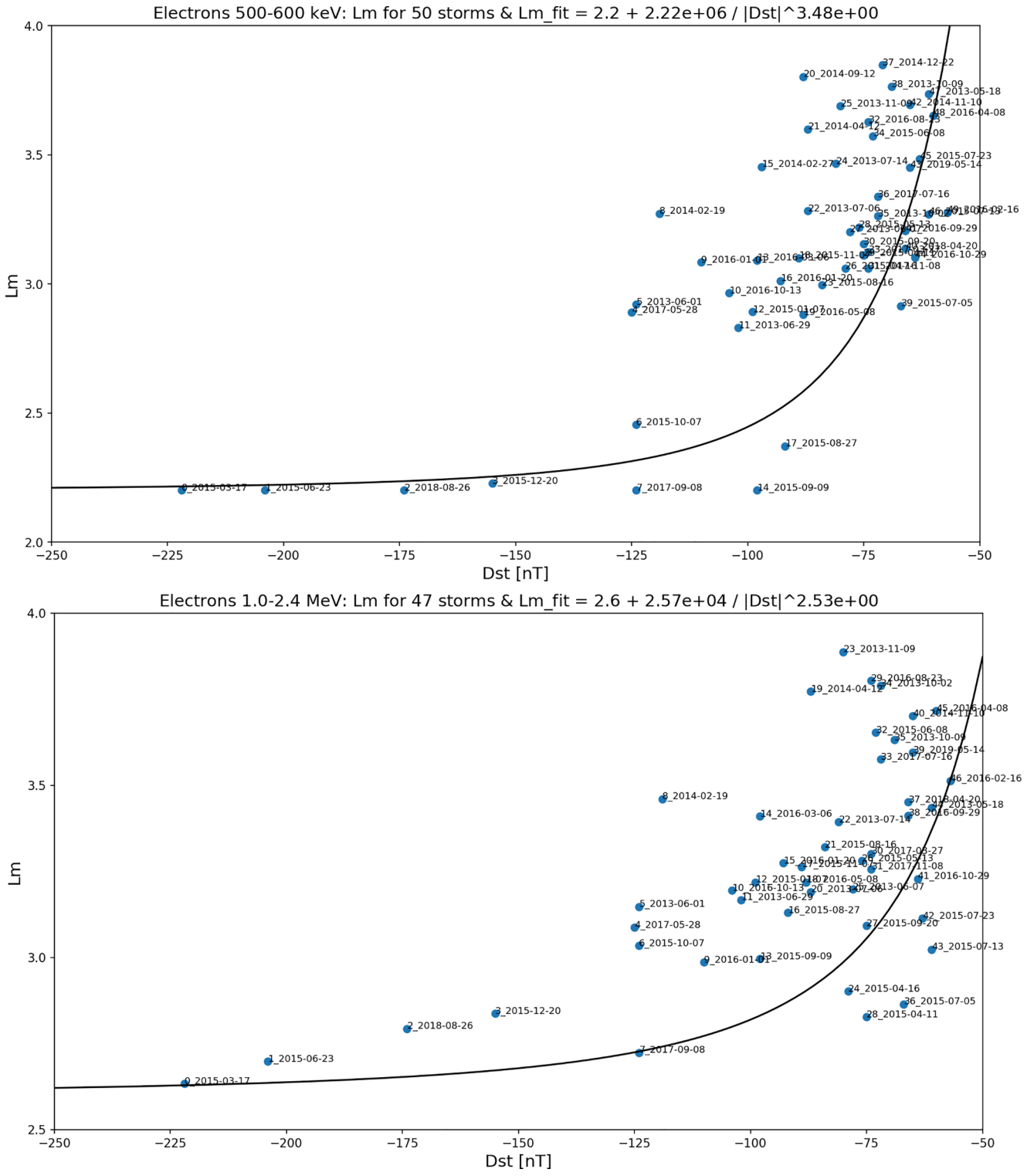

Figure 10. *L*m of the flux injections versus Dst for Ch 1 (500–600 keV, upper panel) and Ch 5 (1–2.4 MeV, bottom panel) for the storms with Dst < −50 nT between May 2013 and December 2019. A nonlinear relation between *L*m and Dst is superposed. Dst, Disturbed Storm Time.

For higher energy 1–2.4 MeV (Ch 5, illustrated in the bottom panel of Figure 10), *L*m does not reach values lower than $L = 2.75$ for the strongest storms observed during this 6-years period. *L*m is slightly higher than for low energies. For < 1 MeV electrons, penetrations into the slot region and inner belt are more frequent

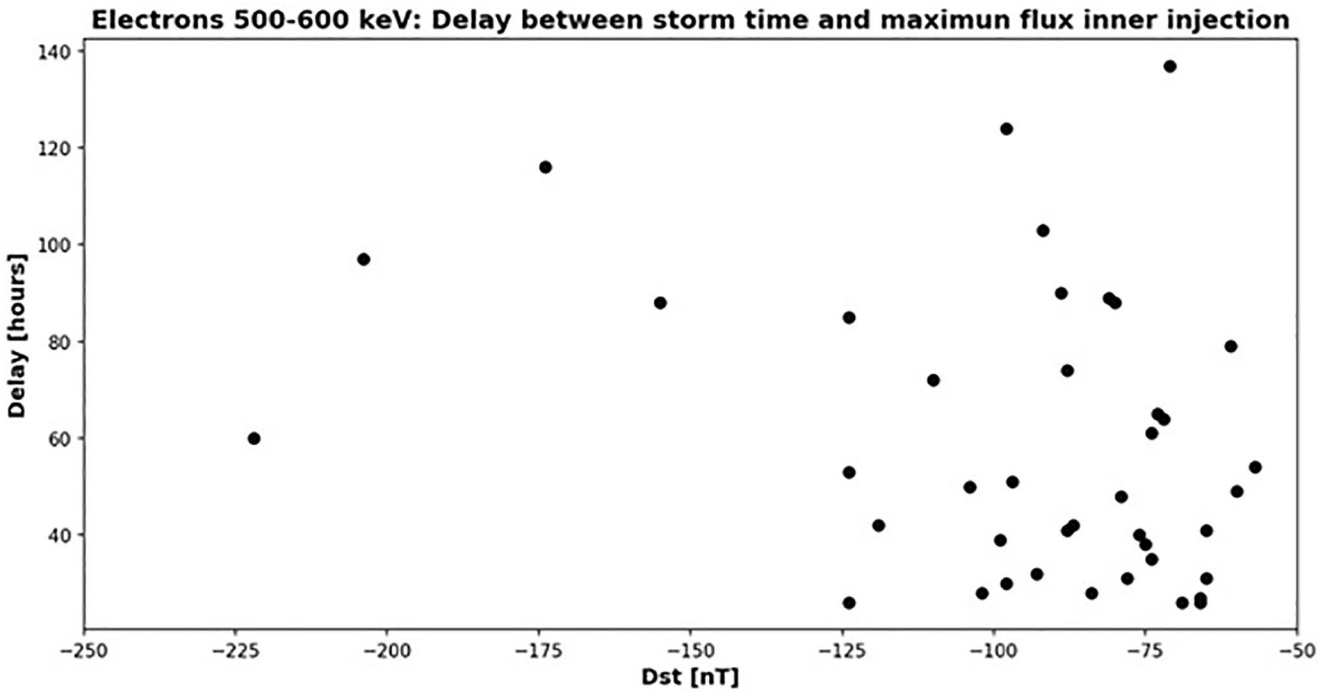

Figure 11. Delay in hours between the time of minimum Dst and the time of maximum flux observed at minimum *L* for the storms recorded for Ch1 electrons. Dst, Disturbed Storm Time.

and also deeper at lower energies than at higher energies. The direct relation between *L*m and Dst is the more obvious for Ch 5, but again, it does not seem to be linear. The relation between *L*m and Dst observed by EPT is better fitted by a power law function (+a constant that corresponds to the lowest *L*m) in both channels. The fitting parameters are reported in the plot titles. The fits are illustrated by the solid line on both panels of Figure 10. They are more realistic than linear relations, especially considering the high variations of *L*m for the weak storms and the almost vertical behavior of the function for very low Dst values, suggesting a threshold or an "impenetrable barrier" as mentioned by Baker et al. (2014) for ultrarelativistic electrons using RBSP data.

Observations from the MagEIS instruments on RBSP show that similar sudden flux enhancements at $L < 2.7$ also appear commonly for 100–200 keV electrons (Turner et al., 2017) and can reach up to 1 MeV. Like in EPT observations, the number of flux enhancement at low *L* decreases with increasing electron energy.

As illustrated in Figure 11, *L*m of the injections appears generally after the minimum of Dst, thus, at the beginning of the recovery phase. Generally, the minimum *L* of flux enhancements appears later (up to 6 days after Dst min) when the minimum of Dst is very low, thus, for strong storms. Note that it takes on average 6 h for solar wind information observed at L1 to be communicated to geostationary orbit inside the magnetosphere (Borovsky et al., 1998) and several hours for Dst to reach its minimum during the main phase of the storm.

4. Radiation Belts—Plasmapause Links

4.1. Observations

A correlation between the inner edge of outer belt and the innermost plasmapause location was first reported by Li et al. (2006) and recently discussed in Khoo et al. (2018). Links between the inner edge of the outer belt and the plasmapause were also identified with previous observations from the LEO satellite SAC-C (Pierrard & Benck, 2012) and with CLUSTER (Darrouzet et al., 2013). Goldstein et al. (2016) quantified the

outer belt and plasmapause position for a 5-day period of 15–20 January 2013 and found that for this event, electron fluxes earthward of belt's peak are anticorrelated with cold plasma density.

It is thus useful to compare the position of the plasmapause with the position of the inner edge of the outer belt observed by EPT, as is done in Figure 13 for Ch 4 (0.8–1 MeV, upper panel) and Ch5 (1–2.4 MeV, middle panel) from 1 March to December 31, 2015.

In Figure 12, the solid black line in the third panel corresponds to the plasmapause position measured by Radiation Belt Storm Probes (RBSP)/Electric and Magnetic Field Instrument Suite and Integrated Science (EMFISIS) and Electric Field and Waves Suite (EFW). The NASA Van Allen Probes (also called RBSP A and B) mission (Mauk et al., 2012) has been launched in 2012 and operated simultaneously with EPT so that both data set. allow to acquire unprecedented studies of the electron radiation belt variability in response to solar activity. RBSP flies on a low inclination (10°) elliptical orbit ranging from 600 to 30,600 km. The Van Allen Probes have two instruments allowing to determine the plasmapause position, the EMFISIS (Kletzing

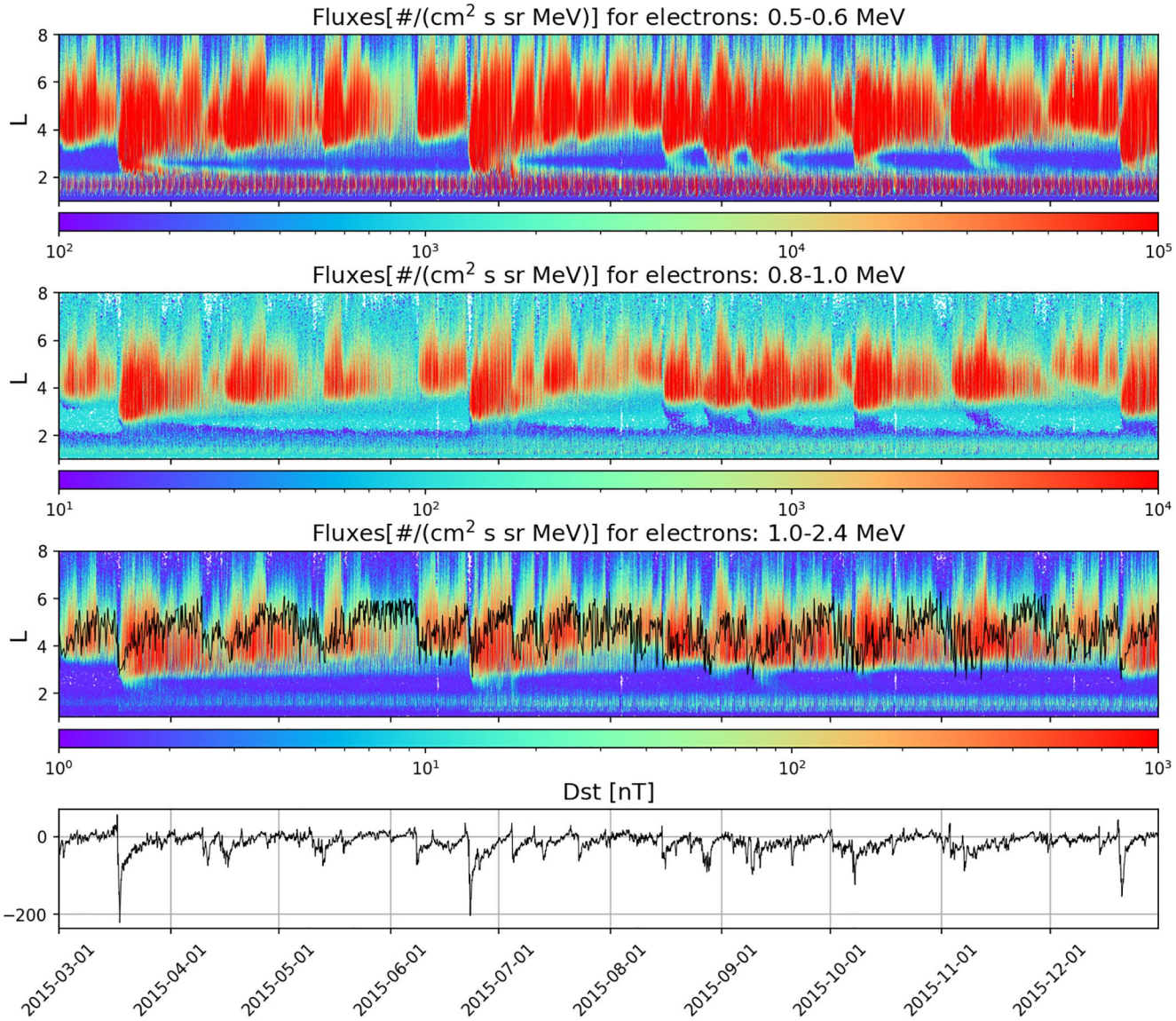

Figure 12. Electron flux measured by EPT in Ch 1 (500–600 keV, upper panel), Ch 4 (0.8–1 MeV, second panel), and Ch5 (1–2.4 MeV, third panel) from March 1 to December 31, 2015. In the third panel, the black line corresponds to the plasmapause position measured by RBSP-B/EMFISIS and EFW. Bottom panel: Dst index during the same period. EFW, Electric Field and Waves Suite; EPT, Energetic Particle Telescope; RBSP-B/EMFISIS, Radiation Belt Storm Probes/Electric and Magnetic Field Instrument Suite and Integrated Science.

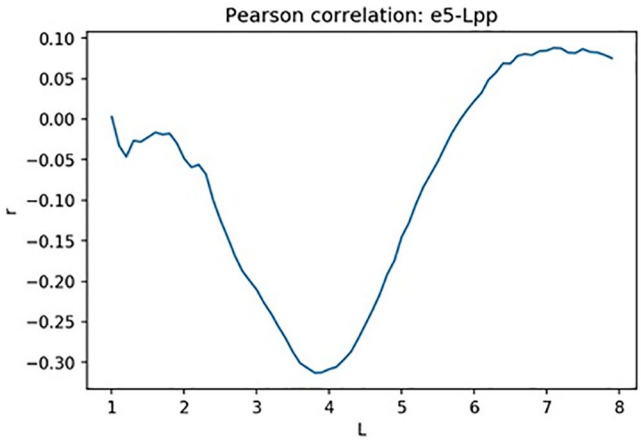

Figure 13. Pearson correlation between the plasmapause position measured by RBSP and the EPT flux in Ch 5 (1–2.4 MeV). EPT, Energetic Particle Telescope; RBSP, Radiation Belt Storm Probes.

et al., 2013), and the EFW (Wygant et al., 2013), delivering simultaneous observations of the radiation belts and the plasmapause.

During moderate and big storms (easily identified by inverted peaks of Dst given in the bottom panel of Figure 13), the plasmapause is formed closer to the Earth and shows an inward motion similar to the inward motion of the inner edge of the outer belt, which appears only for the strongest events. As explained previously in Section 3.3 and illustrated on Figure 12, this inner edge of the outer belt is energy dependent and slightly lower for lower energies. The electron fluxes measured by EPT from September 1, 2013 to May 31, 2014 in Channel 4 (0.8–1 MeV) and Ch5 (1–2.4 MeV) illustrate these effects. Injections in the slot region are clearly visible during storms. The so-called impenetrable barrier (Baker et al., 2014) for ultrarelativistic electrons is also observed from LEO measurements for >2.4 MeV electrons (Pierrard et al., 2019).

The inward motion of the plasmapause during the storm gives a minimum position very close to that of the inner edge of the outer belt for 1 MeV electrons (i.e., Lm [1 MeV], with fit given in Figure 10b). After the storm, the plasmasphere refills in 2 or 3 days, so that the plasmapause is generally much further from the Earth than the inner edge of the outer belt during quiet periods (Pierrard & Voiculescu, 2011).

The inward motion of the outer radiation belt associated with sudden flux enhancements of energetic electrons is directly related to the plasmapause erosion during geomagnetic storms: the closest position of the plasmapause during storms corresponds well to the closest position of the inner edge of the outer belt for electrons with $E = 1$ MeV, suggesting a possible link with the impenetrable barrier for these very energetic electrons. After the storm, the plasmapause moves back to larger radial distances in less than 3 days, while the inner edge of the outer belt remains close to the Earth during more extended periods of several days. This is important since different waves are generated inside and outside the plasmasphere and close to the plasmapause position, all able to contribute to the loss and acceleration of outer belt electrons, therefore changing its edges and spectrum.

Note that the plasmasphere is in corotation with the Earth, while the radiation belt particles drift eastward for electrons and westward for protons with an azimuthal drift velocity that depends on the energy and distance of the particles but is typically several minutes for MeV electrons (e.g. 16 min for a 550 keV electron at $L = 4$)

The Pearson correlation between the plasmapause position measured by RBSP and the EPT flux in Ch 5 (1–2.4 MeV) is illustrated in Figure 13. There is an anticorrelation between the plasmapause position and the flux of energy >1 MeV, appearing around $L = 3.8$–4 where the coefficient of correlation reaches −0.3. These L values correspond to the inner edge of the outer belt for this energy range. Pearson correlations for lower energy channels never reach an absolute value of the correlation coefficient higher than 0.15, showing no correlation for lower energy ranges, as illustrated in Supporting Information S1 for Ch1. More comparisons between EPT and RBSP fluxes will be discussed in a next article.

4.2. Discussion on the Physical Processes

The actual mechanisms responsible for this correlation are still under debate. The two-belt radiation structure has been explained as arising from strong electron interactions with plasmaspheric hiss just inside the plasmapause boundary location (Lyons et al. 1972; Ripoll et al., 2017). Since during strong storms, the plasmasphere is eroded down to low L, local acceleration of MeV electrons by chorus waves can reach the new region outside of the plasmasphere that was previously located in the slot region and inner belt.

It was also suggested that slow natural inward radial diffusion combined with moderate, and persistent, wave-particle pitch angle scattering deep inside the Earth's plasmasphere can combine to create the almost impenetrable barrier through which the most energetic Van Allen belt electrons cannot migrate (Baker et al., 2014). The plasmasphere can then contribute to explain the impenetrable barrier for $E > 2$ MeV.

There are three mechanisms by which the plasmapause may participate to modify the particle fluxes in the outer belt: (i) pitch-angle scattering of electrons by Very Low Frequency (VLF) whistler-mode waves and electromagnetic ion cyclotron (EMIC) waves outside the plasmapause causing them to precipitate; (ii) modification by the plasmasphere of the characteristics of the Ultralow Frequency waves that diffuse particles radially inward in space and up in energy space; and (iii) creation of a peak flux just outside the plasmasphere from acceleration by VLF whistler-mode chorus waves, because those waves are strongest just beyond the plasmasphere.

EMIC waves in the plasmasphere were reported to cause low L-shells nonadiabatic losses at $E > 0.63$ MeV (Bortnik et al., 2006). The dropouts also coincide with the formation of plasmaspheric drainage plumes which favor the development of EMIC waves (Borovsky & Denton, 2009). During quiet periods after storms, the outer belt is inside the plasmasphere, where it endures strong wave-particle interactions causing loss. It is clear that radiation belt populations are sensitive to the core plasmasphere distribution and specifically to the position of the plasmapause.

5. Summary and Conclusions

Using more than 6 years of EPT observations from its launch on PROBA-V in May 2013 to end 2019, we analyzed the influence of the geomagnetic storms with Dst < -50 nT appearing during this period on the electron fluxes with $E > 500$ keV. We showed that at LEO, storms are always characterized by a sharp dropout in the outer belt that appears a few hours before the minimum of Dst, thus, before the end of the main phase. The fluxes disappear at all energies > 500 keV even for weak storms with Dst > -50 nT with a deepness that has been directly related to the value of Dst. Dropouts reach less than $L = 4$, that is, the outer slot region, for the strongest storms. The fluxes then increase during the recovery phase, and contrary to what was observed at GEO orbit in previous studies, the flux is generally higher than just before the storm for all $L < 6$, especially when the successive storms are long time spaced. Indeed, the electron flux slightly decreases with time after the end of the recovery phase, with lifetimes depending on L and energy of typically several days. Only for the strong storms (typically Dst < -50 nT), the dropout is coupled to an injection of new electrons down to lower L-shell, defining a new minimum value Lm for the inner edge of the outer belt that is energy and Dst dependent. Relations have been found between Lmin of the dropout and the Dst index, as well as between the Lm of the injections in the slot and Dst for different energy ranges. For this relation between the minimum of Dst and Lm of injections that appears a few days later, we propose a power law relation, instead of a linear one as given in Li et al. (2017) (their Figure 3), due to the configuration of the observations that suggest a threshold limit for the strongest storms.

The observations of PROBA-V/EPT, confirmed by comparisons with observations of other spacecraft like POES at LEO and RBSP close to the equatorial plane (Pierrard et al., 2014), show that dropouts appear for all energies and all storms, even very weak. The flux enhancements in the slot and inner belt regions appear at energies measured by EPT from 500 keV up to 8 MeV, but with a deepness strongly related to Dst. The most energetic ultrarelativistic particles do not penetrate at $L < 2.6$ during these 6 years and never reach the inner belt, contrary to the lower energy electrons.

Moreover, we have shown in the present paper that during storms, a strong link between the plasmapause and the inner edge of the outer belt is observed, but only for > 1 MeV electrons, in particular in the storm erosion/compression phase that pushes both the plasmasphere and the outer belt together inward.

These investigations are crucial to answer the still unsolved questions of the cause(s) of the dropouts, of the injection mechanism(s), of the process(s) that determine the minimum L value of the penetration and its dependence in energy, and of the links between the plasmapause and the radiation belts. It is only by studying their observed characteristics as a function of L and energy from recent satellite data, more and more reliable due to the improvements of the detectors, that the relative importance of different physical mechanisms can be identified. These observations allow us to better understand which processes are preponderant during the different storms on the dynamic of the radiation belts. Different simulations and theories are compared with the data and investigated in more detail in an upcoming article.

Data Availability Statement

EPT data are publicly available at the ESA website http://swe.ssa.esa.int/space-radiation and RBSP-ECT data (Van Allen Probes) at the website http://www.RBSP-ect.lanl.gov/. Dst are provided on www.spenvis.oma.be.

Acknowledgments
The authors thank the Belgian Science Policy – Space Research and Applications (Belspo) for the support in the scientific analysis of Energetic Particle Telescope (EPT) measurements and for the FEDtWIN project ENERGY. The authors also thank the International Space Sciences Institute (ISSI) and the participants in a 2020 ISSI workshop for the project "Radiation belts physics." V. Pierrard and E. Botek also thank *funding from the Research Executive Agency under the European Union's Horizon 2020 Research and Innovation program (project SafeSpace)*. GC was supported by the Laboratory Directed Research and Development program of Los Alamos National Laboratory under project number 20200073DR. The development of the EPT instrument was realized with the support of Belspo and of the European Space Agency (ESA). The authors thank S. Benck and S. Borisov for validation of the data. The authors thank the EFW and EMFISIS team, in particular, S. A. Thaller, J. R. Wygant, C. A. Kletzing, and W. S. Kurth for the plasma density data that allowed the computation of the plasmapause location in Figure 12.

References

Baker D. N., Jaynes A. N., Hoxie V. C., Thorne R. M., Foster J. C., Li X., et al. (2014). An impenetrable barrier to ultrarelativistic electrons in the Van Allen radiation belts. *Nature*, *515*(7528), 531–534. http://dx.doi.org/10.1038/nature13956

Benck, S., Cyamukungu, M., Cabrera, J., Mazzino, L., & Pierrard, V. (2013). The transient observation-based particle (TOP) model and its potential application in radiation effects evaluation. *Journal of Space Weather and Space Climate*, *3*(A03), 110. https://doi.org/10.1051/SWSC/2013024

Benck, S., Mazzino, L., Cyamukungu, M., Cabrera, J., & Pierrard, V. (2010). Low altitude energetic electron lifetimes after enhanced magnetic activity as deduced from SAC-C and DEMETER data. *Annales Geophysicae*, *28*, 848–859. www.ann-geophys.net/28/849/2010/

Borisov, S., Benck, S., & Cyamukungu, M. (2014). Angular distribution of protons measured by the Energetic Particle Telescope on PROBA-V. *IEEE Transactions on Nuclear Science*, *61*, 6.

Borovsky, J. E., & Denton, M. H. (2009). Relativistic-electron dropouts and recovery: A superposed epoch study of the magnetosphere and the solar wind. *Journal of Geophysical Research*, *114*, A02201. https://doi.org/10.1029/2008JA01312

Borovsky, J. E., Thomsen, M. F., Elphic, R. C., Cayton, T. E., & McComas, D. J. (1998). The transport of plasma sheet material from the distant tail to geosynchronous orbit. *Journal of Geophysical Research*, *103*(20), 297.

Bortnik, J., Thorne, R. M., O'Brien, T. P., Green, J. C., Strangeway, R. J., Shprits, Y. Y., & Baker, D. N. (2006). Observation of two distinct, rapid loss mechanisms during the 20 November 2003 radiation belt dropout event. *Journal of Geophysical Research*, *111*(A12), e2006JA011802. https://doi.org/10.1029/2006JA011802

Claudepierre, S. G., Ma, Q., Bortnik, J., O'Brien, T. P., Fennel, J. F., & Blake, J. B. (2020a). Empirically estimated electron lifetimes in the Earth's radiation belts: 1. Observations. *Geophysical Research Letters*, *47*, e2019GL086053. https://doi.org/10.1029/2019GL086053

Claudepierre, S. G., Ma, Q., Bortnik, J., O'Brien, T. P., Fennel, J. F., & Blake, J. B. (2020b). Empirically estimated electron lifetimes in the Earth's radiation belts: 2. Comparison with theory. *Geophysical Research Letters*, *47*, e2019GL086056. https://doi.org/10.1029/2019GL086056

Claudepierre, S. G., O'Brien, T. P., Looper, M. D., Blake, J. B., Fennell, J. F., Roeder, J. L., et al. (2019). A revised look at relativistic electrons in the Earth's inner radiation zone and slot region. *Journal of Geophysical Research: Space Physics*, *124*, 934–951. https://doi.org/10.1029/2018JA026349

Cunningham, G. S., Botek, E., Pierrard, V., Cully, C., & Ripoll, J.-F. (2020). Observation of high-energy electrons precipitated by NWC transmitter from PROBA-V low-Earth orbit satellite. *Geophysical Research Letters*, *47*, e2020GL089077. https://doi.org/10.1029/2020GL089077

Cyamukungu, M., Benck, S., Borisov, S., Bonnet, J. L., Grégoire, G., Cabrera, J., et al. (2014). The Energetic Particle Telescope (EPT) on board Proba-V: description of a new science-class instrument for particle detection in space. *IEEE Transactions on Nuclear Science*, *61*, 63667–63681. https://doi.org/10.1109/TNS.2014.2361955

Darrouzet, F., Pierrard, V., Benck, S., Lointier, G., Cabrera, J., Borremans, K., et al. (2013). Links between the plasmapause and the radiation belts boundaries as observed by the instruments CIS, RAPID and WHISPER on CLUSTER. *Journal of Geophysical Research: Space Physics*, *118*, 4176–4188. https://doi.org/10.1002/jgra.50239

Goldstein J., Baker D. N., Blake J. B., De Pascuale S., Funsten H. O., Jaynes A. N., et al. (2016). The relationship between the plasmapause and outer belt electrons. *Journal of Geophysical Research: Space Physics*, *121*(9), 8392–8416. http://dx.doi.org/10.1002/2016ja023046

Katsavrias, C., Daglis, I. A., & Li, W. (2019). On the statistics of acceleration and loss of relativistic electrons in the outer radiation belt: A superposed epoch analysis. *Journal of Space Physics*, *124*(4), 2755–2768. https://doi.org/10.1029/2019JA026569

Khoo, L. Y., Li, X., Zhao, H., Sarris, T. E., Xiang, Z., Zhang, K., et al. (2018). On the initial enhancement of energetic electrons and the innermost plasmapause locations: Coronalmass ejection-driven storm periods. *Journal of Geophysical Research: Space Physics*, *123*. https://doi.org/10.1029/2018JA026074

Kletzing, C., Kurth, W., Acuna, M., MacDowall, R., Torbert, R., Averkamp, T., et al. (2013). The Electric and Magnetic Field Instrument Suite and Integrated Science (EMFISIS) on RBSP. *Space Science Reviews*, *179*, 127–181.

Li, X., Baker, D. N., O'Brien, T. P., Xie, L., & Zong, Q. G. (2006). Correlation between the inner edge of outer radiation belt electrons and the innermost plasmapause location. *Geophysical Research Letters*, *33*, L14107. https://doi.org/10.1029/2006GL026294

Li, X., Baker, D. N., Zhao, H., Zhang, K., Jaynes, A. N., Schiller, Q., et al. (2017). Radiation belt electron dynamics at low L (<4): Van Allen Probes era versus previous two solar cycles. *Journal of Geophysical Research: Space Physics*, *122*, 5224–5234. https://doi.org/10.1002/2017JA023924

Lopez Rosson, G., & Pierrard, V. (2017). Analysis of proton and electron spectra observed by EPT/PROBA-V in the South Atlantic Anomaly. *Advances in Space Research*, *60*, 796–805. https://doi.org/10.1016/j.as.2017.03.022

Lyons, L. R., Thorne, R. M., & Kennel, C. F. (1972). Pitch-angle diffusion of radiation belt electrons within the plasmasphere. *Journal of Geophysical Research*, *77*(19), 3455–3474. https://doi.org/10.1029/JA077i019p03455

Mauk, B. H., Fox, N. J., Kanekal, S. G., Kessel, R. L., Sibeck, D. G., & Ukhorskiy, A. (2012). Science objectives and rationale for the Radiation Belt Storm Probes mission. *Space Science Review*, *179*, 1–4. https://doi.org/10.1007/s11214-012-9908-y

McIlwain, C. E. (1966). Magnetic coordinates. *Space Science Review*, *5*, 585–598. https://doi.org/10.1007/BF00167327

Moya, P. S., Pinto, V. A., Sibeck, D. G., Kanekal, S. G., & Baker, D. N. (2017). On the effect of geomagnetic storms on relativistic electrons in the outer radiation belt: Van Allen Probes observations. *Journal of Geophysical Research: Space Physics*, *122*(11), 11–100. https://doi.org/10.1002/2017JA024735

Paulikas, G. A., & Blake, J. B. (1979). Effects of the solar wind on magnetospheric dynamics: Energetic electrons at the synchronous orbit. In W. P. Olson. *Quantitative modeling of magnetospheric processes, geophysical monograph series 21*, (pp. 180–202). Washington, DC: AGU.

Pierrard, V., & Benck, S. (2012). The dynamics of the terrestrial radiation belts and its links to the plasmasphere. in space weather: The space environment. *AIP Conference Proceedings*, *1500*, 216. https://doi.org/10.1063/1.4768769

Pierrard V., Lopez Rosson G., Borremans K., Lemaire J., Maes J., Bonnewijn S., et al. (2014). The Energetic Particle Telescope: First Results. *Space Science Reviews*, *184*(1–4), 87–106. http://dx.doi.org/10.1007/s11214-014-0097-8

Pierrard, V., & Lopez Rosson, G. (2016). The effects of the big storm events in the first half of 2015 on the radiation belts observed by EPT/PROBA-V. *Annales Geophysicae*, *34*, 75–84. https://doi.org/10.5194/angeo-34-75-2016

Pierrard, V., Lopez Rosson, G., & Botek, E. (2019). Dynamics of megaelectron volt electrons observed in the inner belt by PROBA-V/EPT. *Journal of Geophysical Research: Space Physics*, *124*, 1651–1659. https://doi.org/10.1029/2018JA026289

Pierrard, V., & Voiculescu, M. (2011). The 3D model of the plasmasphere coupled to the ionosphere. *Geophysical Research Letters*, *38*, L12104. https://doi.org/10.1029/2011GL047767

Reeves, G. D., McAdams, K. L., Friedel, R. H. W., & O'Brien, T. P. (2003). Acceleration and loss of relativistic electrons during geomagnetic storms. *Geophysical Research Letters*, *30*(10), e2002GL016513. https://doi.org/10.1029/2002GL016513

Ripoll, J.-F., Claudepierre, S. G., Ukhorskiy, A. Y., Colpitts, C., Li, X., Fennell, J., & Crabtree, C. (2020). Particle dynamics in the earth's radiation belts: Review of Current research and open questions. *Journal of Geophysical Research: Space Physics*, *125*, e2019JA026735. https://doi.org/10.1029/2019JA026735

Ripoll, J.-F., Reeves, G. D., Cunningham, G. S., Loridan, V., Denton, M., Santolík, O., et al. (2016). Reproducing the observed energy-dependent structure of Earth's electron radiation belts during storm recovery with an event-specific diffusion model. *Geophysical Research Letters*, *43*(11), 5616–5625. http://dx.doi.org/10.1002/2016gl068869

Ripoll, J.-F., Santolík, O., Reeves, G. D., Kurth, W. S., Denton, M. H., Loridan, V., et al. (2017). Effects of whistler mode hiss waves in March 2013. *Journal of Geophysical Research: Space Physics*, *122*(7), 7433–7462. http://dx.doi.org/10.1002/2017ja024139

Ripoll, J.-F., Loridan, V., Denton, M. H., Cunningham, G., Reeves, G., Santolík, O., et al. (2019). Observations and Fokker-Planck Simulations of the L-Shell, Energy, and Pitch Angle Structure of Earth's Electron Radiation Belts During Quiet Times. *Journal of Geophysical Research: Space Physics*, *124*(2), 1125–1142. http://dx.doi.org/10.1029/2018ja026111

Selesnick, R. S. (2015). Measurement of inner radiation belt electrons with kinetic energy above 1 MeV. *Journal of Geophysical Research: Space Physics*, *120*, 8339–8349. https://doi.org/10.1002/2015JA021387

Turner, D. L., O'Brien, T. P., Fennell, J. F., Claudepierre, S. G., Blake, J. B., Jaynes, A. N., et al. (2017). Investigating the source of near-relativistic and relativistic electrons in Earth's inner radiation belt. *Journal of Geophysical Research: Space Physics*, *122*(1), 695–710. http://dx.doi.org/10.1002/2016ja023600

Turner, D. L., Kilpua, E. K. J., Hietala, H., Claudepierre, S. G., O'Brien, T. P., Fennell, J. F., et al. (2019). The response of Earth's electron radiation belts to geomagnetic storms: Statistics from the Van Allen Probes era including effects from different storm drivers. *Journal of Geophysical Research: Space Physics*, *124*, 1013–1034. https://doi.org/10.1029/2018JA026066

Turner, D. L., O'Brien, T. P., Fennell, J. F., Claudepierre, S. G., Blake, J. B., Kilpua, E. K. J., & Hietala, H. (2015). The effects of geomagnetic storms on electrons in Earth's radiation belts. *Geophysical Research Letters*, *42*(21), 9176–9184. https://doi.org/10.1002/2015GL064747

Turner, D. L., Shprits, Y. Y., Hartinger, M. D., & Angelopoulos, V. (2012). Explaining sudden losses of outer radiation belt electrons during geomagnetic storms. *Nature Physics*, *8*(3), 208–212. https://doi.org/10.1038/NPHYS218

Wygant, J. R., Bonnell, J. W., Goetz, K., Ergun, R. E., Mozer, F. S., Bale, S. D., et al. (2013). The Electric Field and Waves Instruments on the Radiation Belt Storm Probes mission. *Space Science Reviews*, *179*(1), 183–220.

Xiang, Z., Tu, W., Li, X., Ni, B., Morley, S. K., & Baker, D. N. (2017). Understanding the mechanisms of radiation belt dropouts observed by Van Allen Probes. *Journal of Geophysical Research: Space Physics*, *122*, 9858–9879. https://doi.org/10.1002/2017JA024487

Zhao, H., & Li, X. (2013). Modeling energetic electron penetration into the slot region and inner radiation belt. *Journal of Geophysical Research: Space Physics*, *118*, 6936–6945. https://doi.org/10.1002/2013JA019240